January - February 2020
ISSN: 0193-4120 Page No. 16421 - 16435

Numerical Solution for Stagnation Point Flow of a Maxwell Fluid Over a Stretched Surface with Thermal and Concentration Buoyancy Effects

M. Sreedhar Babu[1], V. Venkata Ramana[2], G. Ravi Sankar [3]

[1,2,3]Department of Applied Mathematics, Y.V. University, Kadapa, A.P.

Article Info
Volume 82
Page Number: 16421 - 16435
Publication Issue:
January-February 2020

Article History
Article Received: *18 May 2019*
Revised: *14 July 2019*
Accepted: *22 December 2019*
Publication: *28 February 2020*

Abstract

The motivation behind this introduction is to ponder the numerical reproduction of the stagnation point stream of a Maxwell liquid past an extending surface presented to heat and solutal lightness impacts. Numerical solutions have been determined through the Runge-Kutta-Gill method (RK Gill). Similarity solutions are calculated and presented graphically for non-dimensional velocity, temperature, and concentration, local rate of heat and mass transfer with pertinent parameters. Validation of results is achieved by comparison with earlier results for clear fluid studies. It is found that heat and mass transfer rates are reduced in the assisting flow region and the opposite results were observed due to increment in fluid Deborah number. Such issues have a few applications in engineering and petroleum industries, for example, electroplating, substance handling of heavy metals and solar water heaters.

Keywords:*Maxwell fluid, heat and mass transfer, buoyancy force, RK-Gill method.*

I. INTRODUCTION

For quite a while, basic contemplations have been given to exploring the persistent movement of clingy, incompressible fluids driven by surfaces that broaden straightforwardly through delicate fluids. Such present circumstances are knowledgeable about a few current procedures, for example, cooling metal sheets in cooling showers, streamlined release of plastic sheets, polymer sheets that are reliably released from shading, moving warmth treatment materials, and so on. The It has the quality to proceed onward a perpetual surface between the feed roller and the lap roller or on the vehicle line. During the assembling procedure of these sheets, the blend acquired from the slice is consequently extended to accomplish the perfect thickness. This sheet is at last settled while experiencing an effectively controlled cooling edge to at long last form a great component. Clearly, the properties of the sheet are enormously influenced by heat and mass trade between the sheet and the fluid. During the assembling procedure, the extended sheet is thermally and precisely associated with the encompassing fluid. As Karwe and Jaluria have uncovered, examinations of heat development and current fields are fundamental to decide the idea of the most recent aftereffects of such strategies [1, 2]. In his fundamental work in 1961, Sakiadis [3, 4] introduced a review of limit layer flows on an always solid surface moving at a steady speed. When all is said in done, the sheet is relied upon to be non-stretchable, however in different investigations, for example, the polymer business, it is imperative to deal with the stretch sheet as portrayed in the Crane [5]. Dutta and so on [6] inspected the dissemination of the temperature of the current on the sheet spread by heat progress from a uniform divider. Rajagopal and so forth [7] the advancement of the viscoelastic fluid on the lengthening sheet was examined.

Published by: The Mattingley Publishing Co., Inc.

January - February 2020
ISSN: 0193-4120 Page No. 16421 - 16435

Numerous specialists have looked into a few factors of the present purpose of past stagnation. Ishak and so on [8] examined the two-dimensional MHD stagnation direct current to a sheet spreading with variable surface temperature utilizing the Keller box numerical structure. Ali et al. researched the stagnation ebb and flow of the coupled MHD coupled convection of an incompressible thick fluid that is electrically arranged on a vertical level plate [9]. In their examination [8, 9], numerical position was gathered utilizing an obvious restricted complexity plot. Ali et al. [10] have finished a numerical investigation of the persistent non-straight 2D laminar stream at the MHD stagnation point and the warmth move of the thick incompressible fluid toward the stretch sheet. The investigation thought about captivating and appealing fields, clingy dissemination, and radiation impacts. A numeric course of action was made utilizing a restricted separation methodology. Al-Sudais [11] utilizes a terminating system to create a numerical report exploring the impacts of variable heat conductivity and heat source/sink on the current in the MHD boundary layer of a viscous fluid, which is right around a stagnation point did expandable non-understanding sheet. Ibrahim et al. utilized a fourth Runge-Kutta fourth order method and terminating strategy [12] analyze the impacts of appealing fields on stagnation point flows and heat developments by extending sheets. Mahapatra and so forth [13] utilized a dispatch procedure to explore the impact of a uniform sidelong magnetic field on the two-dimensional current of the stagnation purpose of an incompressible electro rheological gooey fluid on the development surface. Mohammed and so forth, they played out a numerical assessment of the progression of stagnation focuses on a versatile sheet with convective limit conditions.[14] Use of shooting system. Nandy [15] has arrived on the MHD stale stream and an exploratory game plan of the heat development of the Casson fluid on the stretchable seat during the run. In this investigation, a precise course of action was made utilizing a homotopy testing technique. Agbaje et al. they utilized a ghost annoyance technique and a standardization system from a different universe. [16] Dissect the impacts of warmth source/endotherm and suction/infusion of stagnation current toward the extending sheet.

As of late, boundary layer flows for Newtonian and non-Newtonian fluids, metallurgical administration, and the marvels of transport of material development (paints, gels, consumable), creation of discharged fluid polymers, wraps and sheets. The exchange of seeds, heat and vitality takes on significant work in such a strategy. Polymer sheets can be stretched in specific manners to improve mechanical properties by doping with different materials and afterward hot stacking [17]. Non-Newtonian fluids show up in a wide scope of plan structures including oils, remedial lynching suspensions, chemicals, froths, biotechnology liquids and then some. Rosali et al. [18] considering the progression of stagnation indicates where heat moves a stretchy porous sheet. They found that there was a twofold concurrence on case contracts. Qasim [19] inspected the synchronous impacts of heat and mass trade on Jeffreys' non-Newtonian viscoelastic fluid stream, considering heat sources/sinks. Mukhopadhyay [20] analyzed the current in the polarization limit layer with heat move through an exponentially broadening sheet in a thermally stratified medium. He saw that while thinking about the impacts of heat stratification, the pace of heat move expanded while the size of the speed profile diminished because of a higher gauge of alluring parameters. Khalili and so forth [21] accepted a powerless current in a stagnation nanofluid with heat move through a versatile sheet put in a penetrable medium affected by an appealing field. They found that the expansion of alluring parameters, porousness parameters, and speed disseminations expanded the double design space while staying stable for different appraisals of the solid volume of nanoparticles. Furthermore, they have discovered that the porosity parameter influences the current and heat stream from the nanofluid when contrasted

January - February 2020
ISSN: 0193-4120 Page No. 16421 - 16435

with alluring parameters. At that point, Khalili and so forth [22] considered MHD results for nanofluid stream at the stagnation purpose of a penetrable permeable plate that grows/contracts. They considered three kinds of nanoparticles, for example, copper, alumina, and titanium dependent on water. What's more, we found that the skin lattice coefficient and the quantity of Nusselt expanded in each of the three cases to get a higher gauge of the nanoparticle volume. Bhatti et al. [23] A numerical investigation of Maxwell's fluid course through a porous sheet contracted utilizing a dynamic linearization methodology was performed. Shahid et al. [24] researched Maxwell's viscoelastic ebb and flow on an extended permeable sheet utilizing the Cattaneo-Christov warm change model. Gangadhar et al. [25] Using the Cattaneo-Christov heat change theory, the heat conduct of the MHD Carreau fluid over the extension chamber was researched numerically. Gangadhar et al. [26] another world rewind procedure was utilized to disintegrate the nanofluid on the chamber stretched out with the Cattaneo-Christov heat change speculation. As of late, Gangadhar et al [27] and so on they analyzed the impacts of manufactured reaction and convection conditions on hyperbolic surplus liquids past a predictable broadened surface.

Mulling over the examinations referenced over, the reason for the present examination is to analyze the impact of lightness consequences for stagnation point stream of a Maxwell liquid past an extended surface. The overseeing arrangement of incomplete differential conditions is non-dimensionalized and changed into conventional differential conditions and tackled numerically by utilizing the RK-Gill technique. The figures are contrasted and the accessible outcomes in a constraining way. The impacts of included parameters on the speed, temperature and fixation fields are dissected and examined.

II. MATHEMATICAL FORMULATION

Consider a laminar limit layer two-dimensional stagnation point stream of incompressible, upper-convicted Maxwell liquid past an extending surface with heat and solutal lightness impacts. The surface agrees with the plane $\bar{y} = 0$ of a Cartesian co-ordinates as appeared in Fig. 1. The extending surface has straight speed u_w while the speed of the stream outside to the limit layer is u_e. Two equivalent and inverse powers are presented along the x-axis so the sheet is extended with a speed corresponding to the good ways from the cause. The extending surface has a uniform Temperature $\bar{T}_w$ and the free stream temperature is $\bar{T}_\infty$ with $\bar{T}_w > \bar{T}_\infty$. Additionally, it has a uniform focus $\bar{C}_w$ and the free stream fixation $\bar{C}_\infty$ is with $\bar{C}_w > \bar{C}_\infty$.

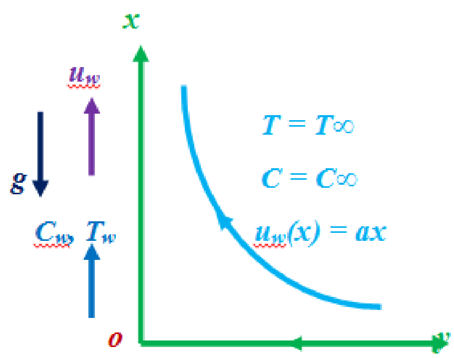

(a) Assisting flow

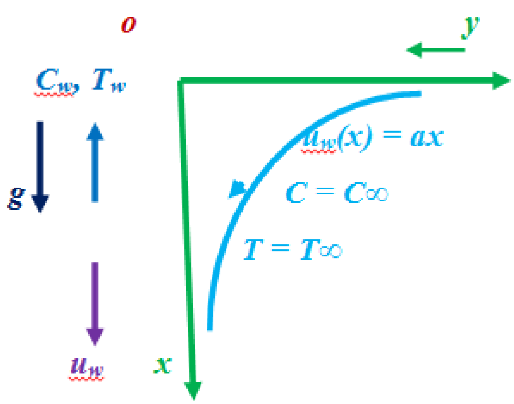

(b) Opposing flow

Fig. 1: Physical model and coordinate system

Published by: The Mattingley Publishing Co., Inc.

$$\frac{\partial \bar{u}}{\partial \bar{x}} + \frac{\partial \bar{v}}{\partial \bar{y}} = 0 , \qquad (1)$$

$$\bar{u}\frac{\partial \bar{u}}{\partial \bar{x}} + \bar{v}\frac{\partial \bar{u}}{\partial \bar{y}} + \lambda_1 \left(\bar{u}^2 \frac{\partial^2 \bar{u}}{\partial \bar{x}^2} + \bar{v}^2 \frac{\partial^2 \bar{u}}{\partial \bar{y}^2} + 2\bar{u}\bar{v}\frac{\partial^2 \bar{u}}{\partial \bar{x}\,\partial \bar{y}} \right) = u_e \frac{du_e}{dx} + \frac{\mu}{\rho}\frac{\partial^2 \bar{u}}{\partial \bar{y}^2} \pm g\beta_T (T - T_\infty) \pm g\beta_C (C - C_\infty), \qquad (2)$$

$$\bar{u}\frac{\partial \bar{T}}{\partial \bar{x}} + \bar{v}\frac{\partial \bar{T}}{\partial \bar{y}} = \alpha \frac{\partial^2 \bar{T}}{\partial \bar{y}^2}, \qquad (3)$$

$$\bar{u}\frac{\partial \bar{C}}{\partial \bar{x}} + \bar{v}\frac{\partial \bar{C}}{\partial \bar{y}} = D\frac{\partial^2 \bar{C}}{\partial \bar{y}^2}, \qquad (4)$$

Here the velocity components denotes $\bar{u}$ and $\bar{v}$ along the $\bar{x}$ - and $\bar{y}$ - directions, respectively. The kinematic viscosity is $\nu = \mu / \rho$, the viscosity of the fluid is μ, the fluid relaxation time is λ_1, the fluid density is ρ, the fluid heat capacity is c_p, and thermal diffusivity is $\alpha = k / \rho c_p$, here the thermal conductivity is k.

The boundary conditions in the present problem are

$$\bar{u} = u_w(\bar{x}) = c\,\bar{x},\ \bar{v} = 0,\ \bar{T} = \bar{T}_w(\bar{x}) = \bar{T}_\infty + b\bar{x},\ \bar{C} = \bar{C}_w(\bar{x}) = \bar{C}_\infty + d\bar{x}, \quad \text{at } \bar{y} = 0 \qquad (5)$$

$$\bar{u} \to u_e(\bar{x}) = a\bar{x},\ \bar{T} \to \bar{T}_\infty,\ \bar{C} \to \bar{C}_\infty, \text{ as } \bar{y} \to \infty \qquad (6)$$

In the above equation, *a, b, c, d* are the constants.

By using these transformations, we have

$$\xi = \sqrt{\frac{c}{\nu}}\,\bar{y},\ \psi = \sqrt{\nu c}\,\bar{x}\,f(\xi),\ \theta(\xi) = \frac{\bar{T} - \bar{T}_\infty}{\bar{T}_w - \bar{T}_\infty},\ \phi(\xi) = \frac{\bar{C} - \bar{C}_\infty}{\bar{C}_w - \bar{C}_\infty} \qquad (7)$$

In which the stream function is ψ, equations (2) - (4) can be reduced to a system of two coupled ordinary differential equations as follows:

$$\frac{\partial^3 f}{\partial \xi^3} - \left(\frac{\partial f}{\partial \xi}\right)^2 + \frac{\partial f}{\partial \xi}\frac{\partial^2 f}{\partial \xi^2} + \frac{a^2}{c^2} + \beta\left(2f\frac{\partial f}{\partial \xi}\frac{\partial^2 f}{\partial \xi^2} - f^2\frac{\partial^3 f}{\partial \xi^3}\right) \pm \lambda\theta \pm \delta\phi = 0 \qquad (8)$$

$$\frac{1}{\Pr}\frac{\partial^2 \theta}{\partial \xi^2} + f\frac{\partial \theta}{\partial \xi} - \frac{\partial f}{\partial \xi}\theta = 0 \qquad (9)$$

$$\frac{1}{Sc}\frac{\partial^2 \phi}{\partial \xi^2}\phi'' + f\frac{\partial \phi}{\partial \xi} - \frac{\partial f}{\partial \xi}\phi = 0 \qquad (10)$$

Here the prime denotes the derivative with respect to ξ. The Prandtl number is given as $\Pr = \nu / \alpha$, where thermal diffusivity is α. The Deborah number is $\beta = \lambda_1 a$, fluid relaxation time λ_1, and the thermal buoyancy parameter is $\lambda = \frac{Gr}{\mathrm{Re}_x^2}$, $Gr = \frac{g\beta_T(\bar{T}_w - \bar{T}_\infty)\bar{x}^3}{\nu^2}$ is the local thermal Grashof number, the solutal buoyancy parameter is $\delta = \frac{Gc}{\mathrm{Re}_x^2}$, $Gc = \frac{g\beta_C(\bar{C}_w - \bar{C}_\infty)\bar{x}^3}{\nu^2}$ is the local solutalGrashof number, and the Schmidt number is $Sc = \nu / D$. The boundary conditions for equations (6) and (7) are

TEST Engineering & Management

January - February 2020
ISSN: 0193-4120 Page No. 16421 - 16435

$$f(0)=0\ ,\ \frac{\partial f(0)}{\partial \xi}=1,\quad \theta(0)=1,\quad \phi(0)=1, \tag{11}$$

$$\frac{\partial f(\infty)}{\partial \xi}\to\frac{a}{c},\quad \theta(\infty)\to 0,\qquad \phi(\infty)\to 0, \tag{12}$$

The physical amounts of intrigue are the skin erosion coefficient C_f, nearby Nusselt number Nu and neighborhood Sherwood number Sh, which are characterized as

$$C_f=\frac{\tau_w}{\rho u_w^2},\ Nu=\frac{\bar{x}q_w}{k(T_w-T_\infty)},\ Sh=\frac{\bar{x}q_m}{D(C_w-C_\infty)}, \tag{13}$$

Here surface shear stress τ_w, the surface heat flux q_w and the surface mass flux q_m are given by

$$\tau_w=\mu\left(\frac{\partial \bar{u}}{\partial \bar{y}}\right)_{\bar{y}=0},\quad q_w=-k\left(\frac{\partial \bar{T}}{\partial \bar{y}}\right)_{\bar{y}=0},\quad q_m=-D\left(\frac{\partial \bar{C}}{\partial \bar{y}}\right)_{\bar{y}=0} \tag{14}$$

With μ are dynamic viscosity, k and D being thermal and mass conductivity's. Using similarity transformations (7), we obtain

$$\sqrt{\mathrm{Re}_x}\,C_f=\frac{\partial^2 f(0)}{\partial \xi^2}\,f''(0),\ \frac{Nu}{\sqrt{\mathrm{Re}_x}}=-\frac{\partial\theta(0)}{\partial \xi},\ \frac{Sh}{\sqrt{\mathrm{Re}_x}}=-\frac{\partial\phi(0)}{\partial \xi}, \tag{15}$$

Where $\mathrm{Re}_x=\frac{a\bar{x}^2}{\upsilon}$ is local Reynolds nomber.

3.1 Solution procedures using the shooting method:

The nonlinear differential conditions (8)– (10) subject to the limit conditions (11)- (12) are of the third request in f and of the second request in θ and ϕ . These conditions are numerically tackled by utilizing the fourth-request Runge–Kutta–Gill strategy coordinated with the shooting system and Newton–Raphson technique. We define

$$f=Y_1,\ \frac{\partial f}{\partial \xi}=Y_2,\ \frac{\partial^2 f}{\partial \xi^2}=Y_3,\ \theta=Y_4,\ \frac{\partial\theta}{\partial \xi}=Y_5,\ \phi=Y_6,\ \frac{\partial\phi}{\partial \xi}=Y_7 \tag{16}$$

We also define the following:

$$\frac{\partial f}{\partial \xi}=F_1,\ \frac{\partial^2 f}{\partial \xi^2}=F_2,\ \frac{\partial^3 f}{\partial \xi^3}=F_3,\ \frac{\partial\theta}{\partial \xi}=F_4,\ \frac{\partial^2\theta}{\partial \xi^2}=F_5,\ \frac{\partial\phi}{\partial \xi}=F_6,\ \frac{\partial^2\phi}{\partial \xi^2}=F_7 \tag{17}$$

Substitute conditions (16) and (17) into conditions (8) - (10), these conditions are decreased to an arrangement of nine concurrent conditions of the main request as pursues:

$$F_1=Y_2, \tag{18}$$

$$F_2=Y_3, \tag{19}$$

$$F_3=Y_2^2-Y_1Y_3-\beta(2Y_1Y_2Y_3-Y_1^2F_3)\mp\lambda Y_4\mp\delta Y_6, \tag{20}$$

$$F_4=Y_5, \tag{21}$$

$$F_5=\Pr(Y_2Y_4-Y_1Y_5), \tag{22}$$

$$F_6=Y_7, \tag{23}$$

$$F_7=Sc(Y_2Y_6-Y_1Y_7), \tag{24}$$

The boundary conditions given in (11) and (12) are replaced by

$$Y_1(0)=0,\ Y_2(0)=1,\ Y_4(0)=1,\ Y_6(0)=1, \tag{25}$$

Published by: The Mattingley Publishing Co., Inc.

January - February 2020
ISSN: 0193-4120 Page No. 16421 - 16435

$$Y_2(\xi_\infty) = a/c,\ Y_4(\xi_\infty) = 0,\ Y_6(\xi_\infty) = 0, \tag{26}$$

Here, ξ_∞ is selected as $\xi_\infty = 10$, depending on the set of the physical parameters.

The obscure beginning conditions are indicated by $Y_3(0) = \zeta,\ Y_5(0) = t$ and $Y_7(0) = s$. We utilize the Newton–Raphson technique to discover ζ, t and s with the end goal that the arrangements of conditions (18)- (26) fulfill the external limit condition (25) – (26). For this situation, we start with the underlying assessment esteems $(\zeta(0),\ t(0),\ s(0))$ by the shooting strategy. The Newton–Raphson calculations extended to incorporate fractional subsidiaries regarding every factor's measurement. This would yield the subsidiary of $F(F_1, F_2, \ldots, F_5)$ as for ζ, t and s as pursues:

$$F_\zeta(F_6, F_7, \ldots F_{10}),\ \ F_t(F_{11}, F_{12}, \ldots F_{15}),$$
$$F_t(F_{16}, F_{17}, \ldots F_{20}), \tag{27}$$

In this way, we have to discover $F_\zeta = 0,\ F_t = 0,\ F_s = 0,$ at the same time. Following Cebeci and Keller [28], this yield an arrangement of mathematical conditions which fulfill the limit conditions when ξ=0.

$$f'_\zeta \zeta + f'_t t + f'_s s + f' = 0, \theta_\zeta \zeta + \theta_t t + \theta'_s s$$
$$+ \theta = 0,\ \ \phi_\zeta \zeta + \phi_t t + \phi'_s s + \phi = 0$$
(28)

Rearranging the system in equation (28) yields a matrix equation AX = B:

$$\begin{bmatrix} f'_\zeta & f'_t & f'_s \\ \theta_\zeta & \theta_t & \theta_s \\ \phi_\zeta & \phi_t & \phi_s \end{bmatrix} \begin{bmatrix} \zeta \\ t \\ s \end{bmatrix} = \begin{bmatrix} -f' \\ -\theta \\ -\phi \end{bmatrix} \tag{29}$$

This grid condition can be explained by Cramer's standard. The following estimate of ζ, t and s can be registered by utilizing the accompanying recipe:

$$\zeta^{(new)} = \zeta^{(old)} + \frac{\det(A_B(I,J))}{\det(A)},$$
$$t^{(new)} = t^{(old)} + \frac{\det(A_B(I,J))}{\det(A)},$$
$$s^{(new)} = s^{(old)} + \frac{\det(A_B(I,J))}{\det(A)} \tag{30}$$

When the estimations of ζ, t and s are known, we utilize the fourth-order Runge-Kutta-Gill strategy to settle the principal request of first order differential conditions F1, $F_{2,\ldots\ldots}$, F_{20}. Following Gill [29], the Runge-Kutta equation is

$$Y_{i+1} = Y_i + \frac{1}{6}hk_1 + \frac{1}{3}\left(\frac{2-\sqrt{2}}{2}\right)hk_2$$
$$+ \frac{1}{3}\left(\frac{2+\sqrt{2}}{2}\right)hk_3 + \frac{1}{6}hk_4, \tag{31}$$

$$k_1 = F(Y_i) \tag{32}$$

$$k_2 = F\left(Y_i + \frac{h}{2}k_1\right) \tag{33}$$

$$k_3 = F\left(Y_i + \frac{1}{2}\left(-1+\sqrt{2}\right)k_1 + \left(1-\frac{\sqrt{2}}{2}\right)k_2\right) \tag{34}$$

$$k_3 = F\left(Y_i - \frac{\sqrt{2}}{2}k_2 + \left(1+\frac{\sqrt{2}}{2}\right)k_3\right) \tag{35}$$

Here h is signified as the progression size. In the present work, the progression size of h = 0.01 is seen as palatable in acquiring the numerical arrangements. For assembly, the greatest total relative distinction between two emphases is utilized inside a pre-allotted resistance $\varepsilon < 10^{-6}$. In the event that the distinction meets the assembly criteria, the arrangement is expected to have joined and the iterative procedure is ended.

Published by: The Mattingley Publishing Co., Inc.

January - February 2020
ISSN: 0193-4120 Page No. 16421 - 16435

3.2Validation of the Numerical Procedure:

With the end goal of approval, the outcomes were contrasted and recently announced outcomes on comparable subjects. The correlation of explanatory outcomes given here is made with the current writing for the specific estimations of stream parameters. These correlations are shown in Tables 1, 2 and 3. The correlation has been palatable and seen as great concurrence with the current outcomes and with insignificant blunders.

IV. COMPUTATIONS AND DISCUSSION:

The changed force condition (8), vitality condition (9) and species condition (10) exposed to the limit states of condition (11) and (12) were numerically comprehended by methods for the Runge – Kutta – Gill technique. Numerical calculations have been introduced for different estimations of the parameters included specifically and Sc that portray the stream attributes, heat and mass transfer and the outcomes are accounted for as far as diagrams and tables. In figs 2-17 The following data is generally utilized (unless otherwise stated): Pr = 7, $\beta = 0.01,\ a/c = 1, \lambda = 0.5,\ \delta = 0.5$, and Sc = 2.62.

Figure 2 shows that the variety of the even speed part with good ways from the surface for different estimations of a/c. It is seen that the limit layer is framed when the extending speed is not exactly the free stream speed for example a/c > 1 for both the instances of helping and restricting streams. For a/c > 1, the stressing movement close to the stagnation locale increments in this way, the speeding up of the outer stream builds which prompts a reduction in the thickness of the limit layer with increment in a/c and therefore, expanding the level speed. This reality was tentatively affirmed by Flachsbart (Schlichting [30]). It is additionally obvious from this figure an altered limit layer is framed when the extending speed hatchet of the surface surpasses the free stream speed hatchet (for example a/c < 1), in helping and contradicting streams.

Figures 3 shows that the impact of the versatility parameter β on the speed profiles for helping and contradicting streams other parameter are kept at steady Pr = 7, $a/c = 0.2,\ \lambda = 0.5,\ \delta = 0.5$, and Sc = 2.62. The versatile power vanishes when β = 0 and the liquid turns into a Newtonian liquid. From Figure 3, it is seen that with the expansion of β, the speed conveyance shows diminishing conduct for the two streams. Physically, higher β shows more grounded thick power which limits the smooth movement, and along these lines the speed diminishes.

The impact of the heat lightness parameter λ and solutal lightness parameter δ on the dimensionless speed profiles is represented in Figures 4 and 5. The positive estimations of the heat/solutal lightness parameter compares to a helping stream past the extending surface, while the negative estimations of the heat/solutal lightness parameter relates to a contradicting stream past the extending surface. In the helping stream, the speed conveyance all through the limit layer increments. In the contradicting stream, the greatness of speed profile diminishes in the limit layer district at all focuses.

Figure 6 outlines the speed profiles for the impacts of Prandtl number Pr on force limit layer for both helping and contradicting streams. Liquid speed diminishes with expanding Prandtl number though the contrary pattern is watched for contradicting stream. Impact of the Schmidt number Sc on speed profiles is appeared in Figure 7 for both helping and contradicting streams. It is obviously seen that speed profiles decline on account of helping stream while the pattern is turned around for contradicting stream.

Figures 8 - 12 show case the assortment of temperature θ(ξ) with ξ for a couple of estimations of a/c, β, λ, δ and Pr. It is seen from Figure 8 that the temperature at a point reduces with increase in a/c for both aiding and negating streams and the estimations of temperature is higher for limiting stream than for helping stream at all core interests. It is in like manner seeing from this figure the

Published by: The Mattingley Publishing Co., Inc.

January - February 2020
ISSN: 0193-4120 Page No. 16421 - 16435

temperature of the fluid decreases as the great ways from the surface is extended. It is moreover observed that as far as possible layer reduces with growing estimation of a/c for both the cases considered in this examination.

Figure 9 shows the temperature profiles for various estimations of (β = 0, 0.3, 0.6) in the by virtue of Deborah number. $\beta = 0$ addresses the sensible fluids (Newtonian fluid). $\beta \neq 0$ addresses non Newtonian Maxwell fluid. For both aiding and negating stream cases, the temperature is found to fabricate as far as possible layer thickness, which achieves augmentation of the temperature profile. Figure 10 frameworks the assortment of temperature θ (ξ) with ξ over an extent of heat limit parameter λ. This figure evidently shows that the temperature profiles decrease with the extension in the estimations of λ for helping stream and, thusly, the lessening of as far as possible layer occurs with the augmentation of λ however this example is exchanged for limiting stream. From Figure 11 it is seen that, for helping stream, the temperature decreases with extending estimations of obsession daintiness parameter δ and pivot design is seen in repudiating stream. The assortments of temperature with ξ over an extent of Prandtl number Pr are depicted in Figure 12. This figure diagrams that as far as possible layer thickness increases with decrease in the estimation of Pr which is connected with an extension in the divider temperature slant and, hereafter, creates an augmentation in the surface heat move rate in both the occurrences of aiding and negating streams. Further, the temperature θ reduces with the extension in Pr. The effects of heat daintiness control are logically enunciated on dimensionless temperature for a fluid with a little Pr.

The assortments in obsession with ξ for various estimations of a/c, β, λ, δ and Sc are showed up in Figures 13 - 17, independently. From Figure 13, it is seen that the obsession lessens with decrease in the estimations of a/c for aiding and repudiating streams. Figure 14 depicts the assortments of obsession profiles with ξ for different estimations of Deborah number β. It is seen that the development of Deborah number β prompts a slight augmentation in the center profiles for aiding and limiting stream. From Figure 15, it is seen that the center reduces with an extension in the estimation of warmth daintiness parameter λ for helping stream and this example is exchanged for confining stream. Figure 16 shows that for helping stream, the obsession reduces with increase in the estimation of center gentility parameter δ. It is moreover observed from this figure the centralization of the fluid decreases as the great ways from the surface augmentations in helping stream. As showed up in Figure 17, the estimation of the dimensionless obsession reduces when the Schmidt number is extended. This result is a direct result of the manner in which that the extension of the Schmidt numbers prompts lessening of as far as possible layers. In like manner, the lessening in the assembly of the fluid prompts a decrease in the fluid speed.

Numerical estimations of the skin grinding coefficient, Nusselt number and Sherwood number against the Deborah number, proportion parameter, Prandtl number and Sherwood number in two cases to be specific helping and restricting stream are introduced in forbidden structure in table 4. It very well may be closed from the table that the estimations of skin grating coefficient increments with an expansion in β and a/c and diminishes with increment in Pr and Sc for helping stream. In contradict stream, the skin grating qualities growth with going up estimations of β, a/c, Pr and Sc. The Nusselt number qualities increment with expanding estimations of a/c and Pr and it is the inverse for and Sc in helping stream. The Sherwood number qualities growth with going up estimations of a/c and Sc and it is the inverse for and Pr in helping stream. The heat and mass transfer esteems are increment as a consequence of increment in β, a/c, Pr and Sc.

Published by: The Mattingley Publishing Co., Inc.

TEST Engineering & Management
January - February 2020
ISSN: 0193-4120 Page No. 16421 - 16435

V. CONCLUSION:

The stagnation point stream of Maxwell liquid precedent an extending surface is considered numerically contained by the sight of lightness impacts. The administering fractional differential conditions were changed into an arrangement of normal differential conditions utilizing closeness change before being explained numerically. The effect of flexibility number β, extending proportion parameter a/c. heat lightness parameter λ, focus lightness parameter δ, Prandtl number Pr, and Schmidt number Sc is inspected. The principle discoveries can be condensed as pursues:

Velocity of the liquid and surface shear pressure increments with an expansion in the benefits of extending proportion parameter for both helping and contradicting streams.

The energy limit layer thickness diminishes though the surfaces shear pressure increments because of increment in the liquid Deborah number.

In a limit layer stream district, liquid speed increments with going up estimations of warm lightness parameter in helping stream and the contrary pattern is watched for restricting stream. Comparable outcomes were seen on account of the fixation lightness parameter.

Fluid temperature and focus decline though surface heat and mass exchange rates increment because of augmentation in the extending proportion parameter for both helping and contradicting streams.

The warm and focus limit layer thickness increments inside the limit stream area with increase in the liquid Deborah number.

The heat and mass exchange rates decline in the helping stream area and the contrary outcomes were seen because of addition in the liquid Deborah number.

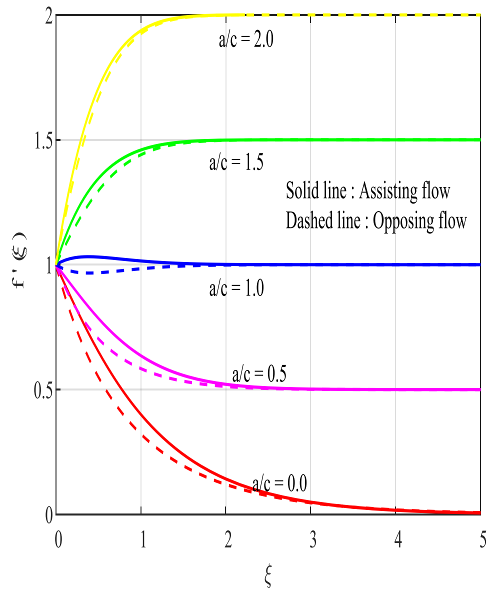

Fig. 2: Velocity distribution $f'(\xi)$ **for special principles of** a/c **for assisting and opposing flows**

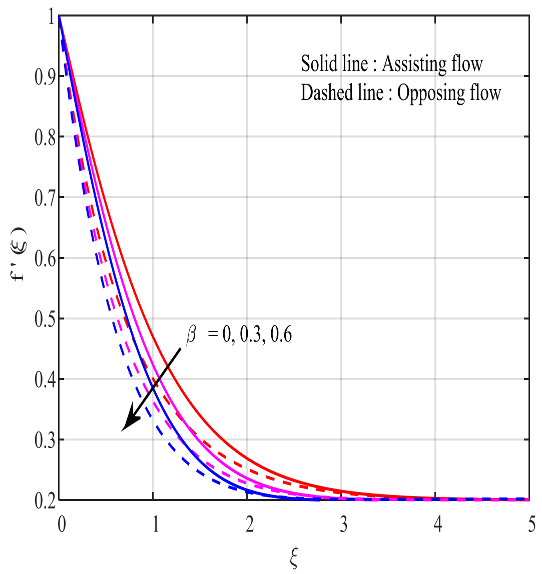

Fig. 3: Velocity distribution $f'(\xi)$ **for special principles of** β **for assisting and opposing flows.**

Published by: The Mattingley Publishing Co., Inc.

January - February 2020
ISSN: 0193-4120 Page No. 16421 - 16435

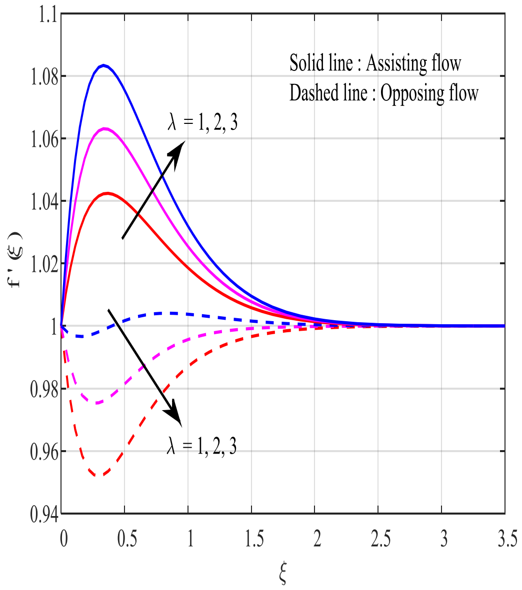

Fig. 4: Velocity distribution $f'(\xi)$ for special principles of λ for assisting and opposing flows.

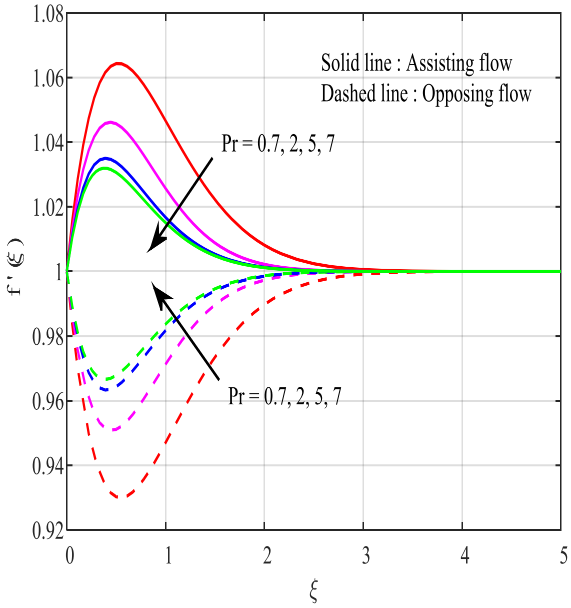

Fig. 6: Velocity distribution $f'(\xi)$ for special principles of *Pr* for assisting and opposing flows for assisting and opposing flows.

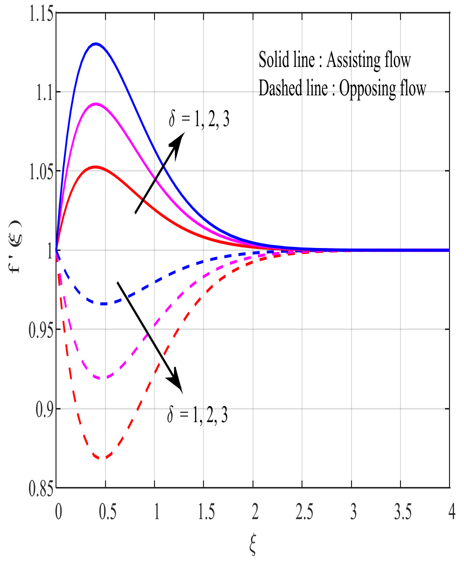

Fig. 5: Velocity distribution $f'(\xi)$ for special principles of δ for assisting and opposing flows.

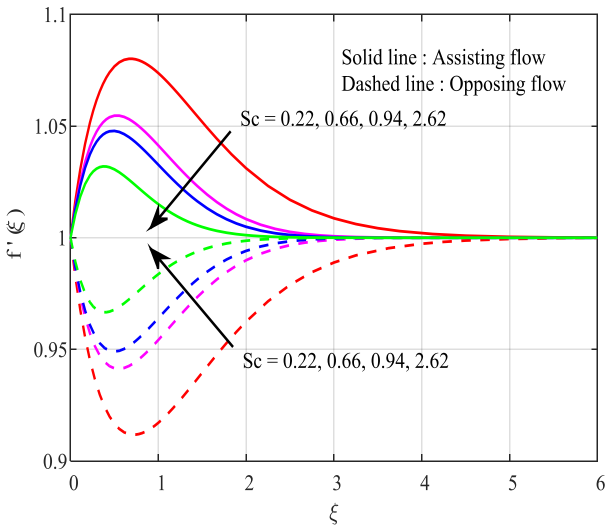

Fig. 7: Velocity distribution $f'(\xi)$ for special principles of Sc for assisting and opposing flows for assisting and opposing flows.

Published by: The Mattingley Publishing Co., Inc.

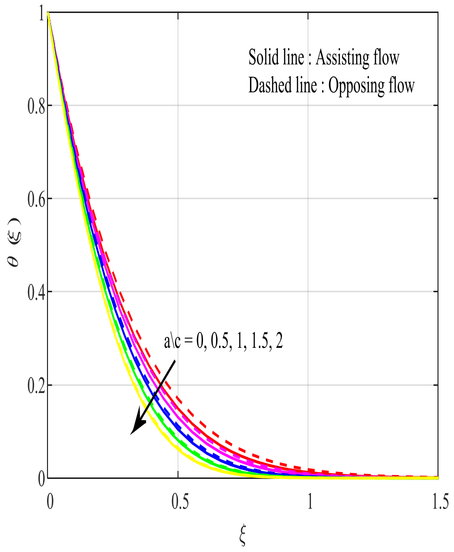

Fig. 8: Temperature distribution $\theta(\xi)$ for special principles of a/c for assisting and opposing flows.

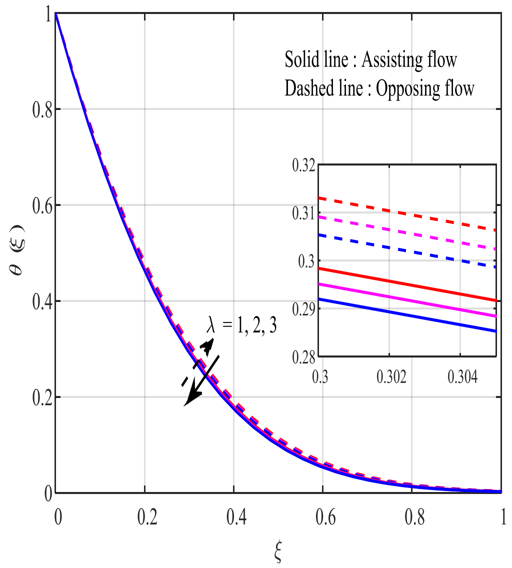

Fig. 10: Temperature distribution $\theta(\xi)$ for special principles of λ for assisting and opposing flows.

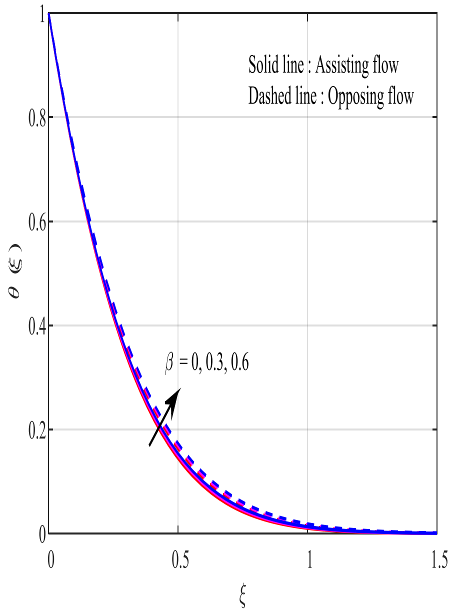

Fig. 9: Temperature distribution $\theta(\xi)$ for special principles of β for assisting and opposing flows.

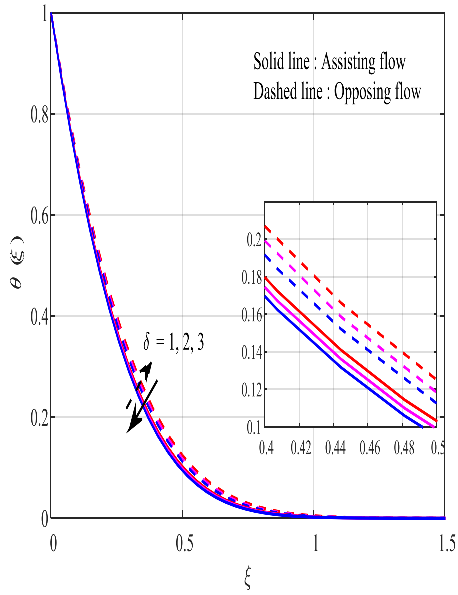

Fig. 11: Temperature distribution $\theta(\xi)$ for special principles of δ for assisting and opposing flows.

Published by: The Mattingley Publishing Co., Inc.

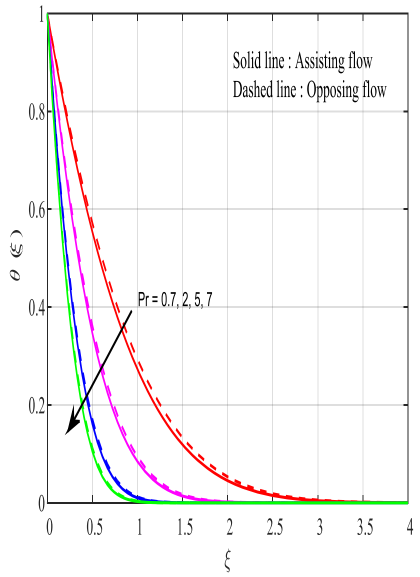

Fig. 12: Temperature distribution $\theta(\xi)$ for special principles of *Pr* for assisting and opposing flows.

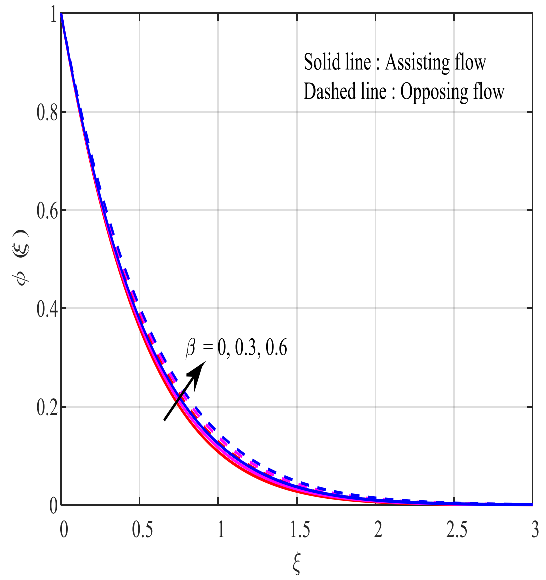

Fig. 14: Concentration distribution $\phi(\xi)$ for special principles of β for assisting and opposing flows.

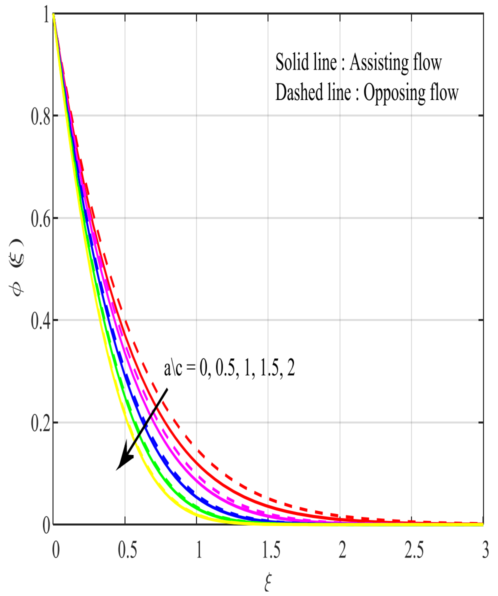

Fig. 13: Concentration distribution $\phi(\xi)$ for special principles of a/c for assisting and opposing flows.

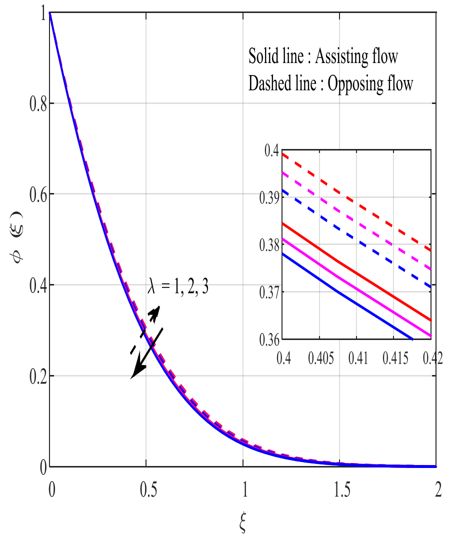

Fig. 15: Concentration distribution $\phi(\xi)$ for special principles of λ for assisting and opposing flows.

Published by: The Mattingley Publishing Co., Inc.

January - February 2020
ISSN: 0193-4120 Page No. 16421 - 16435

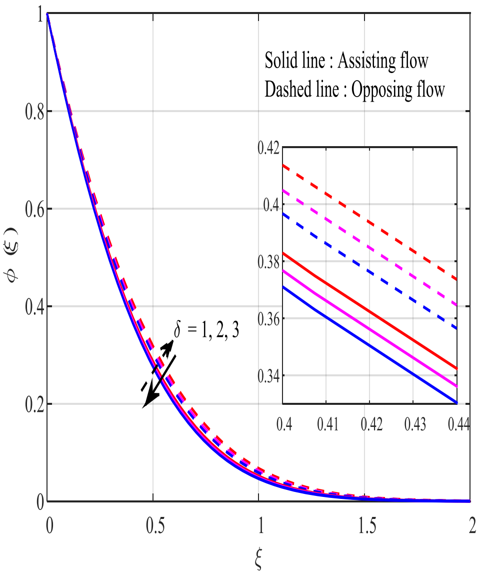

Fig. 16: Concentration distribution $\phi(\xi)$ for special principles of δ for assisting and opposing flows.

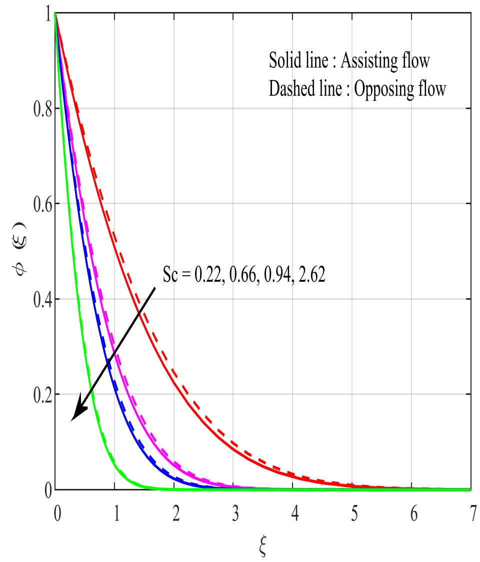

Fig. 17: Concentration distribution $\phi(\xi)$ for special principles of *Sc* for assisting and opposing flows.

Table 1 Relationship of skin friction coefficient $C_f \mathrm{Re}_x^{1/2}$ with the available results in literature for special principles of a/c when *Pr* = *Sc* = 0, $\beta = 0$, $\lambda = \delta = 0$.

a/c	Mahapatra and Gupta [31]	Nazar et al. [32]	Ishak et al. [33]	Pal [34]	Present outcome
0.1	- 0.9694	- 0.9694	- 0.9694	- 0.96939	- 0.969386
0.2	- 0.9181	- 0.9181	- 0.9181	- 0.91811	- 0.918107
0.5	- 0.6673	- 0.6673	- 0.6673	- 0.66726	- 0.667264
2.0	2.0175	2.0176	2.0175	2.01750	2.017503
3.0	4.7293	4.7296	4.7294	4.72928	11.751990

Table 2 Relationship of surface shear stress and local Nusselt number with the available results in literature for special principles of *Pr* when *a/c =1* and *β=0* in the absence of buoyancy force $\delta\phi$ and $\lambda = 1$ for assisting flow.

Pr	Ishak et al. [33]		Pal [34]		Present outcome	
	$C_f \mathrm{Re}_x^{1/2}$	$Nu/\mathrm{Re}_x^{1/2}$	$C_f \mathrm{Re}_x^{1/2}$	$Nu/\mathrm{Re}_x^{1/2}$	$C_f \mathrm{Re}_x^{1/2}$	$Nu/\mathrm{Re}_x^{1/2}$
0.72	0.3645	1.0931	0.36449	1.09311	0.364493	1.093108
6.8	0.1804	3.2902	0.18042	3.28957	0.180415	3.289574
20.0	0.1175	5.6230	0.11750	5.62014	0.117500	5.620131

January - February 2020
ISSN: 0193-4120 Page No. 16421 - 16435

40.0	0.0873	7.9463	0.08724	7.93831	0.087242	7.938306
60.0	0.0729	9.7327	0.07284	9.71801	0.072842	9.718014
80.0	0.0640	11.2413	0.06394	11.21875	0.063942	11.218742
100.0	0.0578	12.5726	0.05773	12.54113	0.057728	12.541100

Table 3 Relationship of surface shear stress and local Nusselt number with the available results in literature for special principles of *Pr* when *a/c =1* and *β=0* in the absence of buoyancy force $\delta\phi$ and $\lambda = 1$ for opposing flow

Pr	Ishak et al. [33]		Pal [34]		Present outcome	
	$C_f Re_x^{1/2}$	$Nu/Re_x^{1/2}$	$C_f Re_x^{1/2}$	$Nu/Re_x^{1/2}$	$C_f Re_x^{1/2}$	$Nu/Re_x^{1/2}$
0.72	- 0.3852	1.0293	- 0.38519	1.02925	- 0.385189	1.029251
6.8	- 0.1832	3.2466	- 0.18323	3.24609	- 0.183232	3.246086
20.0	- 0.1183	5.5923	- 0.11831	5.58960	- 0.118311	5.589598
40.0	- 0.0876	7.9227	- 0.08758	7.91491	- 0.087581	7.914895
60.0	- 0.0731	9.7126	- 0.07304	9.69818	- 0.073041	9.698182
80.0	- 0.0642	11.2235	- 0.06408	11.20118	- 0.064078	11.201180
100.0	- 0.0579	12.5564	-0.05783	12.52519	- 0.057828	12.525150

Table 4 Values of surface shear stress, surface heat and mass transfer rates for special principles of *β*, *a/c*, *Pr* and *Sc* for assisting and opposing flows.

β	*a/c*	*Pr*	*Sc*	Assisting flow			Opposing flow		
				$C_f Re_x^{1/2}$	$Nu/Re_x^{1/2}$	$Sh/Re_x^{1/2}$	$C_f Re_x^{1/2}$	$Nu/Re_x^{1/2}$	$Sh/Re_x^{1/2}$
0.01	1	0.7	0.22	0.418195	1.086313	0.609488	-0.448470	1.003150	0.561847
0.02	1			0.418242	1.086229	0.609388	-0.448441	1.003263	0.561967
0.03	1			0.418518	1.086205	0.609368	-0.448425	1.003372	0.562080
0.04				0.418657	1.086147	0.609304	-0.447875	1.003633	0.562362
0.05				0.417665	1.085795	0.608865	-0.448346	1.003600	0.562313
0.01	0.5			-0.182237	0.989731	0.530082	-1.272395	0.808267	0.418510
	1.5			1.283949	1.186022	0.683905	0.528907	1.133045	0.654406
	2.0			2.363186	1.282208	0.752556	1.683991	1.244493	0.731887

1	1		0.402396	1.294036	0.608131	-0.429550	1.204886	0.563797
	2		0.372706	1.818215	0.605993	-0.394577	1.719357	0.566810
	5		0.337458	2.853046	0.604105	-0.354155	2.745543	0.569379
	7		0.326049	3.367762	0.603635	-0.341360	3.258148	0.569998
	0.7	0.66	0.369618	1.078540	1.047359	-0.391096	1.013895	0.984399
		0.94	0.353715	1.076263	1.246585	-0.372711	1.016903	1.179105
		2.62	0.309786	1.070824	2.065675	-0.322856	1.023870	1.987567

REFERENCES

[1] Karwe MV, Jaluria Y (1988) Fluid flow and mixed convection transport from a moving plate in rolling and extrusion processes. ASME J Heat Transf 110:655–661
[2] Crane LJ (1970) Flow past a stretching plate. Z Angew Math Phys 21:645-647
[3] Dutta BK, Roy P, Gupta AS (1985) Temperature field in flow over a stretching sheet with uniform heat flux. IntCommun Heat Mass Transf 12:89–94
[4] Rajagopal KR, Na TY, Gupta AS (1984) Flow of a viscoelastic fluid over a stretching sheet. RheolActa 23:213-215
[5] Ishak A, Jafar K, Nazar R, Pop I. MHD stagnation point flow towards a stretching sheet. Phys A: Stat MechAppl 2009; 388 (17):3377–83.